Numerical Analysis of Micro-jet Array Cooling Device with Various Configurations

Yang-Ki Jung[a]
Korea Automobile Testing & Research Institute, Samjon-ri, Songsan-myun Hwasung-si, Gyeonggi 445-871, Korea

In-Chan Lee
Memory Research and Development Division, Hynix Semiconductor Inc., Bubal-eup, Icheon-si, Gyeonggi 467-701, Korea

Tae-Young Ma
Department of Electric Engineering, Gyeongsang National University, Gajwa-dong, Jinju-si, Gyeongnam 660-701, Korea

[a]E-mail : hyky89@kotsa.or.kr

(Received November 11 2004, Accepted April 4 2005)

Numerical and visualization procedures are used in a finite difference grid to analyze and better understand the heat transfer in the MEMS based air micro-jet array (MJA) impingement cooling device. The Navier-Stokes (NS) equations with incompressible flow are solved using an implicit procedure. The temperature contour and velocity vector visualization diagrams are used for illustration. The computed temperature distribution at the bottom of the MJA is in good agreement with the experimental measurement data. The parameters are investigated to improve the efficiency of heat transfer in the MJA. The optimum configuration of the MJA is suggested. The present modeling explains the flow phenomenon and yields valuable information to understand the flow and heat transfer in MJA.

Keywords : Micro-jet array, Impinging cooling, Heat transfer, Computational fluid dynamics

1. INTRODUCTION

The cooling of localized, non-uniformly distributed, hot spots on circuit boards remains a significant electronic packaging problem. If the heat removal requirements of these locations are utilized for setting global cooling characteristics, the cooling systems would be overdesigned, leading to unacceptable cost, size, noise and vibration. This is especially true in air-cooled applications such as small computers, communication switching and transmission equipment. Therefore, a preferable design alternative is required to provide the high cooling rates where they are needed. Impinging jets have been reported extensively in the literature because the advantages of the impingement heat transfer process are direct, localized heating or cooling, and increased heat fluxes.

Impingement jet cooling and heating devices have been developed for a long time in many engineering applications. There are abundant articles on the subject of impinging jets[1]. The heat transfer concept of an impinging jet on a solid surface is well known for its high heat transfer coefficient as reported in Wang et al.[2,3]. Gardon and Cobonpue[4] studied the average heat transfer coefficients and the variation of heat transfer coefficients from point to point on the cooled surface. Martin[5] provided an excellent survey of heat and mass transfer under impinging gas jets of empirical correlations accompanied by inviscid analysis for single round and slot jets. A comprehensive survey of jet emphasizing their engineering application is shown in[5]

For decades, air as impinging fluid has been the preferred fluid for cooling electronic packages due to its simplicity, low cost, no inventory problems, no environmental concern, ease of maintenance and more portable. However, as the limits of air-cooling are challenged with the trend of constantly increasing power generation and dissipation, the development of novel cooling devices for very high heat removal rates is in demand. Using air, the highest attainable values for the heat transfer coefficient

for natural and forced convection has been 0.0025 and 0.1 $W/cm^2\,^0C$, respectively from Kim and Lee[6]. Therefore, to overcome the limits of air-cooling, using the same fabrication processes and materials that are used to make microelectronic devices, micro-electro-mechanical systems (MEMS) technology conveys the advantages of miniaturization and integrated electro-mechanical systems. Using MEMS technology, efficient use of air for heat removal in small electronic devices using forced convection requires investigations of miniature air impinging cooling devices. Leland et al.'s[7] micro jet array (MJA) cooler as shown in Fig. 1 is well suited for these applications. They built the MJA air impinging cooling device for high power electronics that combines microscopic scale and impingement. The MJA was constructed from silicon wafers using MEMS technique. They projected that the silicon based micro-jet array air impinging cooler could eventually be machined directly into the die of an electronic device, thereby eliminating much thermal resistance and consequently optimizing the use of air cooling. The MJA achieved the heat transfer coefficient of 0.25 $W/cm^2\,^0C$. Hence, the MJA has been proven as a very efficient cooling device as shown in[7].

We recommend to use MS Word processor and prepare text within the dimensions shown on these pages; In A4 paper, left and right margin are 16 mm respectively, 8 mm middle margin, 35 mm top margin, and 27 mm bottom margin. When a paragraph starts, give an indent of 2 characters. In the last page of the article, make the length of left and right stage to be equal approximately.

Make use of the maximum stipulated length apart from the following two exceptions (i) do not begin a new section directly at the bottom of a page, but transfer the heading to the top of the next column; (ii) you may exceed the length of the text area by one line only in order to complete a section of text or a paragraph.

To be able to utilize this MJA cooler to its fullest capacity and in multiple applications, one has to fully understand the heat transfer process inside the very small and complex geometry of the MJA. However, in reality it is not yet possible to monitor and understand the temperature flux inside the MJA by experimental techniques. To improve heat transfer performance, the designer is faced with the problem of changing many parameters. Therefore, a new approach is necessary to investigate the MJA.

Computational techniques become a valuable tool for the simulation of heat transfer and jet flow. This type of research is significantly less expensive than some experimental techniques and allows more freedom to study different type of jets and jet flow features. Once a computer model is constructed and verified, it can be opti-

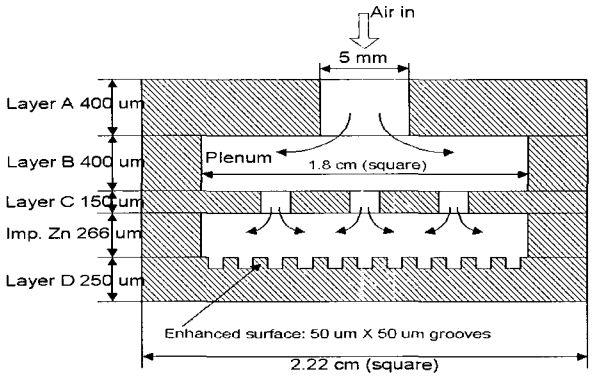

(a) Profile view of the micro-jet array cooler

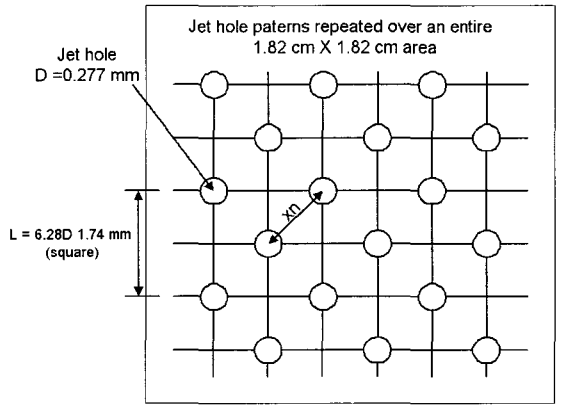

(b) Layer C plan view

Fig. 1. Schematic of the Micro-jet Array Cooler.

mized by implementing and testing hundreds of changes in a short amount of time. In this study, computational fluid dynamics (CFD) is applied to understand the heat phenomenon inside the MJA and enhance heat transfer performance.

There has been no investigation of the numerical work for the flow in a MJA. In this paper our computed results are compared with the experimental measurements in[7].

2. COMPUTER MODELING

Since the grid spacing used is very small, no turbulence models are considered and hence the computation is considered to be by direct numerical simulation method (DNS). As a start, this flow is considered to be incompressible. This assumption imposes a restraint on the upper value of the velocity range that could be tested. Inlet velocities less than 25 m/s are used since they produce maximum velocities $\leq$ 100 m/s, which is the limit for incompressible flow.

2.1 Governing equations

The three-dimensional incompressible Navier-stokes (NS) equations in general tensor notation are as follows:

$$\text{Continuity:}\quad \frac{\partial u}{\partial x}+\frac{\partial v}{\partial y}+\frac{\partial w}{\partial z}=0 \tag{1}$$

$$\text{X-momentum:}\quad \rho\frac{Du}{Dt}=-\frac{\partial P}{\partial x}+\mu\nabla^2 u+\rho f_x \tag{2.a}$$

$$\text{Y-momentum:}\quad \rho\frac{Dv}{Dt}=-\frac{\partial P}{\partial y}+\mu\nabla^2 v+\rho f_y \tag{2.b}$$

$$\text{Z-momentum:}\quad \rho\frac{Dw}{Dt}=-\frac{\partial P}{\partial z}+\mu\nabla^2 w+\rho f_z \tag{2.c}$$

$$\text{Energy:}\quad \rho\frac{DT}{Dt}=\frac{\partial}{\partial x}\left(k\frac{\partial T}{\partial x}\right)+\frac{\partial}{\partial y}\left(k\frac{\partial T}{\partial y}\right)+\frac{\partial}{\partial z}\left(k\frac{\partial T}{\partial z}\right)+\lambda(\nabla)^2+2\mu\nabla^2 \tag{3}$$

Where u, v, and w represent the x, y, and z components of velocity, P is the pressure force, ρ is the density, μ is the molecular viscosity coefficient, k is heat conductivity, λ is the second viscosity coefficient ($\lambda=-\frac{2}{3}\mu$), and f_x, f_y, and f_z are the body forces in x, y, and z components. The details of the derivation are reported in Anderson[8]. Equations (1) and (2) were solved in time until a steady state was reached. Once the velocity field was computed, then the energy equation (3) was solved for the temperature as a steady state equation in space.

All variables are solved at the nodes. The governing equations are approximated either by the finite difference or the finite volume method. Equations (2a, 2b, and 2c) are approximated by central differences. In Equation (3), the convection term is approximated by an upwind procedure while the rest of the terms are approximated by central difference. The NS equations are solved either as steady state using SIMPLE procedure or as unsteady state as in[9]. Due to the complexity of the flow, difficulty in convergence is encountered using steady state procedure. Hence at this time, an unsteady implicit procedure is used. The implicit method used to solve NS equations is the one suggested in Selvam[9]. Implicit treatment of the convective and diffusive terms eliminates the numerical stability restrictions. In this implicit solution procedure, the time step is kept for Courant-Frederick-Lewis (CFL) number less than one.

2.2 Computational grid

MJA cooler is shown in Figs. 1 and 2. Figure 2 shows that air enters the device plenum and is distributed over the orifice plate. The air then flows through the orifice plate creating a high heat transfer zone under each of the 221 jets. Then, the air is exhausted from the two opposite edges of the cooler. More details about the MJA are given in[7]. Only one quarter of the MJA is considered for computer modeling due to symmetry in the horizontal plane. A computer program is written to generate a grid for this complex region. The grid has 324,000 (90×90×40) points. In the vertical direction, an equal spacing of 0.025 mm is used. In the horizontal direction unequal spacing is used to consider the hole and no-hole regions of the plate. The diameter of the hole in the orifice plate is discretized using 5 points.

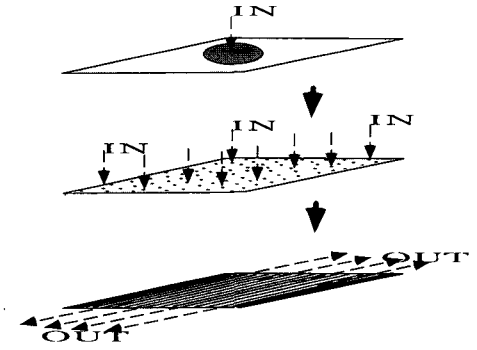

Fig. 2. Schematic of micro-jet array cooler.

2.3 Boundary conditions

The quarter model plan in the x-y plane is shown in Fig. 3. Along boundaries AB and AD, a symmetric boundary condition is imposed. On the wall, a no slip boundary condition is introduced. A velocity of 21 m/s is kept at the 5.0 mm diameter inlet which is equal to the mass flow rate of 0.5 g/s in[7]. The temperature at the inlet is also assumed to be 20 °C. The pressure at the exhaust is considered to be zero, and at all other boundaries where the velocity is known, the normal derivative of the pressure is considered to be zero. The normal derivatives of the velocities are also considered to be zero at the exhaust. The material properties for air are assumed to be as follows: $\nu=10\times10^{-6}$ m^2/s, thermal diffusivity, a = 22×10^{-6} m^2 /s, and cp=0.001 J/(kg-K). The boundary conditions are as follows:

Inlet: $u_{in}=0,\ v_{in}=0,\ w_{in}=21\,m/s,\ T_{in}=20\,^{\circ}\mathrm{C}$

Outlet: $p_{out}=0$

Wall: The viscous flow no-slip conditions are
$u=0,\ v=0,\ w=0$

The adiabatic wall conditions are $\frac{\partial p}{\partial n}=0,\ \frac{\partial T}{\partial n}=0$

At the bottom of the MJA, Leland et al.[7] used 2.31 mm copper plate. At the middle of the copper plate, they

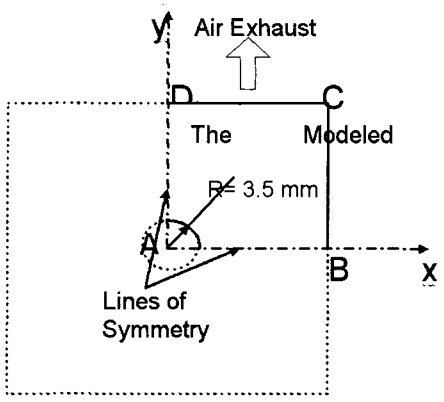

Fig. 3. Solution region and boundary conditions. Top view of the quarter model of the micro-jet array.

embedded the thermocouples. In this analysis, the heat flow rate of 15 W is considered to be at the bottom of the plate. In the current modeling, the grooves in Fig. 1 are not considered due to a lack of refinement in the grid. Instead the thermal diffusivity "a" is increased to 44×10^{-6} m^2/s which is equivalent to the ratio of the grooved area to the plane area times the thermal diffusivity of air. To consider the diffusion in the silicon plate at the bottom of MJA, four extra layers with thickness of 0.025 mm are considered in the solution of temperature distribution. Hence, the grid for temperature solution becomes $84\times84\times54$ points. Since the thermal diffusivity of silicon is very high, it is hard to solve the equations together for both air and silicon. Hence, a value of a $=1000\times10^{-6}$ m^2/s for silicon is used at this time. The diffusion in the copper plate is not considered.

3. RESULTS AND DISCUSSION

The numerical predictions are compared with the experimental date of [7]. In the experiment conducted by [7], they measured the temperatures at 16 points along the bottom plate which are locations of 16 type T 30 AWG thermocouples which were embedded in 0.69 mm hole drilled along the mid-plane of a 2.31 mm thick copper heat spreader. The jet diameter Reynolds number ranged from 456 to 1405. Reynolds numbers are based on the jet characteristics, such as jet exit velocity and jet diameter while others used arrival velocity along with characteristics that they defined as follows:

$$\mathrm{Re} = \frac{V * D}{\nu} \tag{4}$$

The device average heat transfer coefficient was obtained for a variety of heat fluxes to determine the effect of variable properties of the air. A Nusselt number correlation including a correction for variable properties was developed. Determining the Nusselt number is critical to determining the heat transfer coefficient h as shown in Equation (5).

$$h = \frac{Nuk}{D} \tag{5}$$

Leland averaged these temperatures and reported average bottom temperature to be about 57 °C for an input power of 15 W and a flow rate of 0.5 g/s, which is equal to flow velocity of 21 m/s.

3.1 Comparison between numerical and experimental results

In our computer modeling, computed average temperature at the bottom plate is reported to be 54 °C and the heat transfer coefficient is reported to be about 865 W/m^2 K for an input power of 15 W and a flow rate of 0.5 g/s. These results are much closed to Leland's data which is the temperature of 46 °C. The maximum temperature computed in the solution region is 124 °C.

The computed temperature distribution at the bottom of the plate is shown in Fig. 4 and the temperature along the centerline at the exhaust is shown the Fig. 5. A heat patch is spread out in the area between the second and the fifth holes from the center of the jet. This hot patch is due to flow re-circulation occurring between the jets as shown in Fig. 6. The close up view of the re-circulation region between the second and third hole is shown in Fig 7. From this illustration, the re-circulated air retains the heat in those regions; hence a higher temperature distribution is formed at the bottom plate. It explains that multi-jet have the strong interaction between adjacent jets which reduces the stagnation point heat transfer. This may be very hard to measure or visualize using experimentation because the MJA has very small and complicated geometry. However, computer modeling allows us to study and visualize heat and flow transfer inside the MJA. Therefore numerical modeling has proved to be a useful tool in understanding the flow phenomenon inside the MJA.

As shown in Fig. 4 and 5, the temperature near the exhaust is computed to be about 98 °C. However, this high temperature does not exist in the experiment. In the computer modeling, the micro-jets in the orifice plate close to the exhaust are not considered because these holes are very close to the outflow region. Therefore, it is very hard to solve the equations accurately having such a complex flow close to the outflow region. Also, in reality heat can dissipate by convection and radiation at the edges, but these factors are not considered in the computer model.

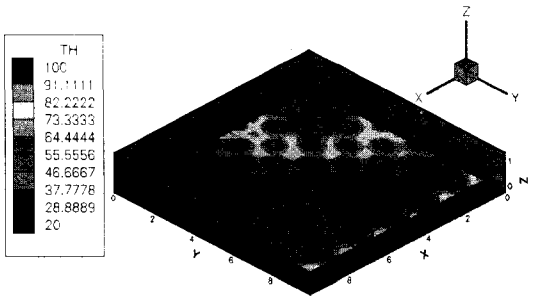

Fig. 4. Contour diagram for temperature at the bottom of the plate.

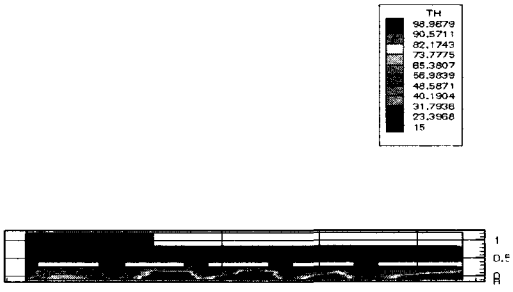

Fig. 5. Contour diagram for temperature along the centerline at the exhaust.

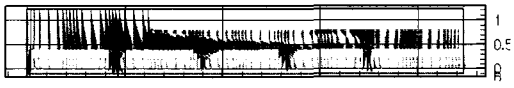

Fig. 6. Velocity vector diagram along the centerline at the exhaust.

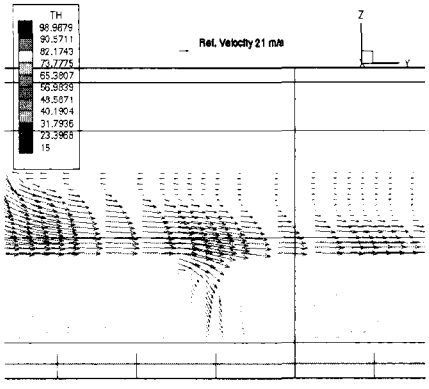

Fig. 7. Close-up view of velocity vector diagram along the centerline at the exhaust around the third hole from the center.

3.2 Improvement of the heat transfer performance

To improve the heat removal capacity, different grids

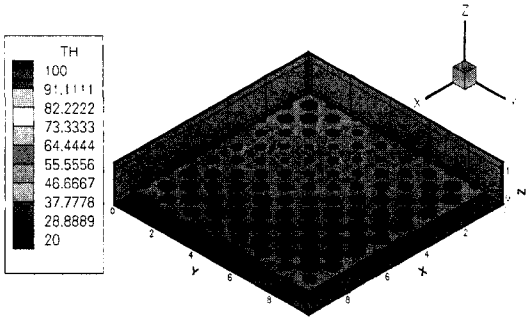

Fig. 8. The best case (case 17).

are used to cover all of the parameters. By changing the distance from the jet to the plate Zn, jet diameter D, jet spacing Xn, and plenum height, various configurations are investigated. The different grids used are illustrated in Table 1 along with all the other boundary conditions and geometric properties.

All the cases covered are compared to each other by computing their heat transfer coefficients and average bottom temperatures. The results are shown in Table 2. Case 17 (optimum case) shows that the computed average temperature at the bottom plate is reported to be 37 °C and the heat transfer coefficient is about 1603 W/m^2K. Standard case (case 3) produces the average temperature at the bottom plate of 54 °C and the heat transfer coefficient of 865 W/m^2K. Case 17 improve the heat transfer performance by approximately 85 % and decreases average bottom temperature by approximately 31 % relative to case 3. The computed temperature distribution at the bottom of the plate is shown in Fig. 8 As seen in Fig. 8 the hot patch phenomenon is greatly removed compared to case 3 shown in Fig. 4.

To increase heat transfer performance of the MJA air impinging cooling device, this research has reached several conclusion as follows:

1. By changing the jet-to-plate distance, heat removal capacity increase as Zn decreases until a value of $Zn = 0.2$ mm is reached.

2. For the investigated impinging jet diameters, the smaller holes yielded better results until D = 0.15 mm is reached.

3. By changing jet-to-jet spacing Xn, heat removal capacity is increased until a ratio $Xn/D \approx 3.5-4.5$ is reached.

4. Heat transfer efficiency increases as plenum height increases until a height of 0.6 mm is reached, and as the jet length decreases until a length of 0.15 mm is reached.

Table 1. The parameters investigated.

Case Number	Description	Parameter Covered
Case 1	W/t layer C	Single jet
Case 2	W/t layer C fewer grid points	
Case 3	Standard Case, D= 0.277 mm, W/t E H, Af = 0.04, .zi/D = 0.96, zp = 0.4 mm	Different jet sizes D with the same Af, zi/D, and zp
Case 4	D= 0.1933 mm	
Case 5	D= 0.1933 mm w/(E H)	
Case 6	D= 0.434 mm	
Case 7	D= 0.277 mm	Af = 0.08
Case 8	D= 0.1933 mm w/(E H)	
Case 9	D= 0.434 mm	
Case 10	Standard Case	Different input velocities
Case 11	Standard Case	
Case 12	D=0.1933 mm w/ (E H)	
Case 13	Zi/D =0.5	Different impinging height ratio zi/D
Case 14	Zi/D =1.5	
Case 15	Zp= 0.3 mm	Different Plenum height zn
Case 16	zp= 0.6 mm	
Case 17	D = 0.1933, Af =0.04 w/ (EH), zi/D= 0.5 zp=0.6	Combination of the best parameters

Table 2. Results.

Case #	Max Heat °C	Avg Temp °C	$\bar{h}$ W/m² K	D Avg $\overline{Nu_D}$	Avg imp. $\overline{V_e}$ m/s	D Avg $\overline{\mathrm{Re}_D}$ No	Max exit V m/s	Location X Y Z in mm Of Max. V
1	165	79	463	77	21	4950	47	2.07X2.77X0.075
2	211	89	392	65	21	4946	37	2.275X1.82X0.0625
3	86	54	865	8.6	29	382	90	0.939X0.939X0.225
4	89	42	1264	8.1	37	344	99	1.26X1.26X0.162
5	78	44	1129	7.3	34	318	96	0.60X2.97X0.36
6	120	48	970	14	38	794	92	0.217X2.821X0.58
7	129	67	579	5.3	16	208	79	2.999X0.544X0.45
8	123	65	604	3.9	19	171	85	0.905X0.905X0.162
9	158	75	500	7.2	19	399	82	0.217X2.505X0.600
10	88	51	884	8.2	27	355	78	0.939X0.939X0.225
11	83	48	993	9.2	32	416	106	0.939X0.939X0.225
12	77	41	1270	8.2	40	366	115	0.604X2.972X0.360
13	75	47	1014	9.4	29	377	87	0.8697X2.54X0.300
14	87	50	910	8.4	29	385	91	0.939X0.939X0.35
15	119	55	773	7.1	28	373	104	2.36X1.305X0.45
16	86	45	1113	10.3	30	402	77	0.939X0.939X0.225
17	61	37	1603	10.3	39	361	76	4.181X0.604X0.270

4. CONCLUSION

The flow and heat transfer in the MEMS based the micro-jet array (MJA) air impinging cooling device is computed by solving the incompressible Navier-Stokes (NS) equations. The flow equations are solved by finite difference procedure in a rectangular grid system. A computational grid of about 500,000 points is used to model the flow in the MJA. The computed temperature distribution at the top of the bottom plate is compared with the experimental measurements of [7] for the case of inlet velocity 21 m/s or 0.5 g/s of mass flow rate and 15 Watts of power input. The computed temperature of about 54 °C at locations just below the jets is in reasonable agreement with the measured value of about 57 °C. At the bottom of the plate away from the jet impingement, higher temperature region is noticed from the second to the fifth hole from the center as shown in Figure 4. This unexpected temperature distribution is due to the re-circulating air between the jets. The computer model has yielded this valuable information to understand the flow and heat transfer in MJA.

To improve the heat removal capacity, the optimum configuration is investigated. The computed average temperature at the bottom plate and the heat transfer coefficient are reported to be 37 °C and 1603 W/m^2 K. This optimum case improves heat removal capacity by approximately 85 % and decreases average bottom temperature by approximately 31 % relative to previous case.

REFERENCES

[1] S. J. Downs and E. H. James, "Jet Impingement Heat Transfer-A Literature Survey", American Society of Mechanical Engineers, p. 1, 1987.

[2] X. S. Wang, Z. Dagan, and L. M. Jiji, "Heat transfer between a circular free impinging jet and a solid surface with non-uniform wall temperature or wall heat flux—1. Solution for the stagnation region", Int. J. Heat Mass Transfer, Great Britain, Vol. 32, No. 7, p. 1351, 1989a.

[3] X. S. Wang, Z. Dagan, and L. M. Jiji, "Heat transfer between a circular free impinging jet and a solid surface with non-uniform wall temperature or wall heat flux—2. Solution for the boundary layer region" Int. J. Heat Mass Transfer, Great Britain, Vol. 32, No 7, p. 1361, 1989b.

[4] R. Gardon and J. Cobonpue, "Heat transfer between a flat plate and jets of air impinging on it", International Heat Transfer Conference 2nd Boulder Colo. and Westminster, London, England, International Developments in Heat Transfer; Proceedings New York, p. 454, 1963.

[5] H. Martin, "Heat and mass transfer between impinging gas jets and solid surface", Advances in Heat Transfer, Vol. 13, p. 1, 1977.

[6] S. J. Kim and S. W. Lee, "Air Cooling Technology for Electronic Equipment", CRC Press, Inc. Florida, 1996.

[7] J. E. Leland, R. Ponnappan, and K. S. Klasing, "Experimental Investigation of an Air Micro Jet Array Impingement Cooling Device", AIAA-99-0476, 37th AIAA Aerospace Sciences, Reno, NV, 1999.

[8] J. D. Anderson Jr., "Computational Fluid Dynamics: The Basic with Applications" , McGraw-Hill, 1995.

[9] R. P. Selvam, "Computation of pressures on texas tech university building using large eddy simulation" Journal of Wind Engineering and Industrial Aerodynamics, Vol. 67~68, p. 647, 1997a.